Silane Pyrolysis in a Piston Reactor

A piston reactor has been developed to examine some aspects of particle formation during the pyrolysis of silane (SiH_4). This reactor generates conditions intermediate between a static pyrolysis reactor and a shock tube reactor. It effectively excludes contributions of wall reactions to the pyrolysis experiments. The apparent kinetics for this reactor do not conform to values published in the literature. A model that incorporates silane-particle reactions can account for the deviations. In addition, emission of visible light accompanies the sooting reactions. The source of this emission seems to be the sum of incandescence from the hot particles and continuum radiation from another source.

Philip W. Morrison, Jr.
Jeffrey A. Reimer
Department of Chemical Engineering
University of California
Berkeley, CA 94720

Introduction

The chemistry of silane (SiH_4) plays a fundamental role in the chemical vapor deposition (CVD) of thin films of silicon (Jasinski et al., 1987) and sinterable silicon powders (Alam and Flagan, 1986; Cannon et al., 1982a, b; Wu and Flagan, 1986, 1987; Wu et al., 1987). Because these materials are technologically important, the chemistry of SiH_4 relevant to CVD and ceramic powders continues to receive much attention. One aspect of silane chemistry important to both CVD and powders is the process of particle formation during pyrolysis (sooting) (Cannon et al., 1982a, b; Eversteijn, 1971; Herrick and Woodruff, 1984; Hoschele et al., 1986; Murthy et al., 1976; Steinwandel and Hoeschele, 1985; Wu and Flagan, 1987; Wu et al., 1987). Particle formation remains less understood because silicon nucleation is extremely complicated and a very fast process. Because there is no accurate chemical mechanism for particle formation, sooting is difficult to predict *a priori* in a new CVD reactor design and is difficult to control in powder reactor designs. This manuscript describes work on a new reactor to explore particle formation from SiH_4 pyrolysis.

Understanding the basis of the new design requires some background in silane chemistry. The following equations are a simple description of the chemistry of SiH_4 found in a pyrolytic reactor.

$$SiH_4(g) \xrightarrow[\text{reactions}]{\text{homogeneous}} SiH_2(g) + H_2(g) \xrightarrow[\text{nucleation}]{\text{reactive}} \text{Si soot} \quad (1)$$

$$SiH_4(g) \xrightarrow[\text{reactions}]{\text{heterogeneous}} SiH_x(s) + (2 - x/2)H_2(g) \quad (2)$$

The left side of Eq. 1 is the homogeneous pyrolysis of silane and is understood reasonably well. Many different techniques have been used to study this reaction: static pyrolysis (Neudorffl et al., 1980; Purnell and Walsh, 1966; White et al., 1985), shock tubes (Newman et al., 1979), and laser heating (Jasinski and Estes, 1985). From the above experiments, these authors have determined that

1) The decomposition product is silylene (SiH_2).

2) There is little or no free radical character to the pyrolysis

3) The pyrolysis has an experimental activation energy of 222–235 kJ/mol (the high-pressure activation energy is closer to 250 kJ/mol).

SiH_4 will also react heterogeneously with high-temperature surfaces (>500°C) to form solid silicon-hydrides (Eq. 2). The films deposited above 600°C have little or no hydrogen; below 600°C, the hydrogen content increases rapidly with decreasing temperature. The apparent kinetics of this reaction depends on the type of film being grown: amorphous hydrogenated silicon (Beers and Bloem, 1982), polycrystalline silicon, and single crystal silicon (Hottier and Cadoret, 1983; Donahue and Reif, 1986).

Historically, particle nucleation (right side of Eq. 1) has been the least understood aspect of silane chemistry, but it has been receiving more attention recently as the CVD and ceramic powder technologies mature. Particle nucleation is a nuisance in silane CVD for two reasons:

1) Silicon particles formed in the deposition zone can contaminate the film

2) The high rates of nucleation divert the conversion of SiH_4 from film to particles.

Empirical optimization of the reactor can sometimes reduce the impact of nucleation to acceptable levels, but this generally lowers the deposition rate (<1–10 μm/h).

In contrast, particle nucleation is central to the production of sinterable silicon powders. Ceramic applications require mono-

Current address of P. W. Morrison, Jr.: Advanced Fuel Research, P. O. Box 18343, East Hartford, CT 06118.

disperse, submicrometer particles that are roughly spherical and nonagglomerated. In an ideal reactor, particles would nucleate in a controllable way and then grow to a predetermined size. In practice, however, the threshold for nucleation is very sensitive to gas temperature and SiH_4 partial pressure (Wu and Flagan, 1987). Since spontaneous nucleation and subsequent coagulation produce particles of a broad size distribution (Wu et al., 1988), powder reactors have the same problem as CVD reactors: confining nucleation to specific reactor volumes.

The physics of sooting has been studied experimentally by four different methods:

1) CVD reactors—both thermal and plasma
2) Shock tubes
3) Flow aerosol reactors
4) Laser synthesis reactors

The tools available to the experimentalist include light scattering, optical absorption, optical extinction, electron microscopy, modeling, and particle counters.

Since sooting is endemic to CVD reactors, some of the first experiments have used CVD reactors. Eversteijn (1971) has performed one of the first detailed investigations of particle formation from silane. His work focuses on nucleation in a hot tube reactor operating at roughly 1,000°C and atmospheric pressure; the feed stock is typically 0.1% SiH_4 in H_2. Eversteijn has derived the following empirical relationship for nucleation in a SiH_4/H_2 mixture:

$$\ln P_{crit} = + (164\ \text{kJ/mol})/RT - 18.1 \qquad (3)$$

where

P_{crit} = critical partial pressure of silane, torr
R = ideal gas constant
T = absolute gas temperature, K

Other authors provide additional descriptions of the sooting process. Murthy et al. (1976) have investigated particles that form in a horizontal epitaxial reactor. The operating conditions are similar to those used by Eversteijn. According to electron microscopy, the particles are 300–800 Å (30–80 nm) in size and are crystalline. The average size of the particles increases with temperature, and the total particle mass increases with silane partial pressure and temperature. Van den Brekel and Bollen (1981) find similar results in their low-pressure CVD reactor (SiH_4 in N_2). The onset of particle nucleation is very sensitive to silane partial pressure: laser scattering from particles increases 2–3 orders of magnitude by changing the partial pressure less than 13.3 Pa (0.1 torr).

Roth and Spears, and their coworkers have studied light scattering by particles in a plasma CVD reactor (Roth et al., 1985; Spears et al., 1986). The plasma reactor is a radio frequency discharge typically using $<10\%$ SiH_4 in Ar. Using a dye laser operating at 500 nm, Roth et al. (1985) observe large scattering intensities at the sheath near both electrodes. The peak intensities increase with increasing pressure and decreasing SiH_4 fraction. The widths of these peaks also vary with pressure and SiH_4 fraction. Flow rate has a complicated effect on the particle scattering intensity.

Steinwandel and coworkers probe the sooting chemistry with shock tubes. They employ a gas mixture of 1% SiH_4 in Ar, and final temperatures of 1,250–3,000 K; the ultimate silane partial pressure never exceeds 3 torr (0.4 kPa). These investigators avoid temperatures $<1,200$ K, because hydrodynamic equations do not accurately predict the temperature of such a weak shock. Optical extinction detects particle formation, and optical emission spectroscopy observes the thermally induced fluorescence of the gas mixture (Steinwandel and Hoeschele, 1985). The spectra of shocks above 3,000 K indicate that Si, Si_2, SiH, and SiH_2 are present; at shock temperatures near 7,000 K, the emission spectra include contributions from H and H_2. The optical extinction measurements show the presence of particles when the temperature is below 2,500 K. Presumably, higher temperatures simply evaporate the particles and form the observed $Si(g)$. The intensity of the extinction varies inversely with the probe wavelength, indicating the particle size is smaller than the wavelengths of visible light (Rayleigh extinction). Particle extinction (and therefore particle number density) is a *strong* function of supersaturation (Hoschele et al., 1986), and high temperatures and low silane partial pressures reduce sooting. The extinction usually appears within 50 μs of shock heating; the shock itself lasts 100–300 μs.

Flagan and coworkers (Alam and Flagan, 1986; Wu and Flagan, 1986, 1987; Wu et al., 1987, 1988) use a flow aerosol reactor to study particle growth and size distribution. A seed reactor pyrolyzes a mixture of 1% SiH_4 in N_2 to produce a large number of seed particles for the growth reactor. Before entering the growth reactor, the seeds are mixed with additional $SiH_4 + N_2$ to dilute the particle number density and add more reactant. To prevent nucleating new particles, the temperature increases parabolically along the length of the reactor. At the input to the growth reactor, the silane concentration is highest and the temperature is kept low to maintain a low supersaturation. As the particles grow, the silane concentration falls, and the larger particles are increasingly effective scavengers of condensible vapors. As a result, the temperature (and pyrolysis rates) can be increased down the length of the reactor (Alam and Flagan, 1986). Wu et al. (1987) use series of rate balances and a simple collisional theory to describe the growth of an n-mer from monomer up to its final particle size (typically 0.1 μm). Efficient computational algorithms make this possible. The only chemical step in this model is the production of monomer from silane; collisional rates (not chemistry) control the subsequent growth of the n-mer. Wu et al. assume that the monomer is SiH_2 and use the kinetics of White et al. (1985). Such a detailed model accurately predicts the final particle size distribution in the seed reactor.

Wu and Flagan (1987) also have used the growth reactor to pinpoint the transition from growth on a seed particle to spontaneous nucleation of new particles. The effectiveness of seeds as nucleation inhibitors is a function of seed number density and seed size. Consequently, Wu and Flagan vary the number density and size of the seeds to determine the nucleation threshold as a function of flow rate, silane concentration and temperature. The transition from growth on the seeds to catastrophic nucleation is extremely abrupt. A 17% change in the silane concentration causes a 10^4 increase in the number of particles. The clusters (n-mers) that fuel the catastrophic nucleation must be very small (~ 0.01 μm) to account for the fast growth rates.

Cannon et al. (1982a, b) have developed a laser synthesis reactor to produce Si, Si_3N_4, and SiC powders. In this reactor, SiH_4 flows upward through a tube and enters the reaction zone; a coannular flow of Ar confines the silane to the central core of the laminar flow. Passing a CO_2 laser beam across the flow causes the SiH_4 to absorb infrared radiation from the laser.

Because the vibrational relaxation times of SiH_4 are long, collisions among the SiH_4 molecules thermalize the absorbed energy and the local gas temperature rises. This configuration generates a visible flame above the laser beam, and the resultant particles form a plume within and above the flame. The particles are about 0.05 μm in size and are crystalline. Typical conditions are: peak gas temperature of $\approx$1,300 K; total pressure of 2×10^4 Pa (150 torr); 10 cm^3/min of SiH_4; and 1,000 cm^3/min of Ar. Cannon et al. (1982a, b) have used optical emission, brightness spectrometry, and thermocouples to estimate the gas temperature, but they do not believe any of these methods are very accurate. Except for this fact, the laser reactor has excellent spatial control over particle nucleation and avoids possible contamination from the walls of the reactor.

The design of the piston reactor reflects the goal of examining reactor conditions different from flow pyrolysis, shock tubes, aerosol reactors, and laser synthesis. In a high-temperature flow pyrolysis, much of the silane heterogeneously pyrolyzes on the hot furnace walls (for example, Scott et al., 1984), and this generates H_2 that dilutes the gas phase and exerts an uncontrollable chemical influence on the homogeneous pyrolysis. The heterogeneous pyrolysis also depletes the gas phase of SiH_4. In a shock tube, the reaction time is short (100–300 μs), and this makes it difficult to observe the nucleation reactions. Shock tubes are also rather sophisticated and can be used only at high pressures. The major drawback of laser synthesis is that the gas temperature is not accurately known. The operation of the aerosol reactor does not allow any interpretation of the kinetics of growth; only size distribution can be examined.

The piston reactor (Morrison and Reimer, 1987) avoids many of these problems. The concept is very simple: a piston in a cylinder compresses a mixture of 1% SiH_4 in noble gas to high temperatures ($\approx$1,000 K) until the SiH_4 decomposes; the cylinder walls remain at a low temperature ($\approx$500 K) because of their large heat capacity. The low wall temperature prevents heterogeneous decomposition of SiH_4. The transport processes are also slow enough to prevent the loss of intermediates on the reactor walls [e.g., $SiH_2(g)$]. The reaction time (1–10 ms) is much longer than in a shock tube, and a wide variety of temperatures is possible by adjusting the wall temperature and final conditions. Monitoring the pressure and volume of the reactor as functions of time yields a good measure of the time dependence of the temperature.

Experiments with the piston reactor show that the only detectable deposits on the piston walls are silicon particles. Particles form in every experiment where there is a detectable conversion of SiH_4. These particles are submicrometer in size, and their hydrogen content decreases as the reaction temperature increases. The formation of particles also generates visible light whose sources are the hot, incandescing soot and some other emitter of continuum radiation. The presence of the hot soot can substantially increase the expected conversion beyond what would be predicted by SiH_2 formation kinetics. A model accounts for the increased conversion by including growth on the particle surfaces.

Experimental Description

A previous manuscript describes the reactor in detail (Morrison and Reimer, 1987), and we only review the principles here (Figure 1). The reactor is a 30-cm-long cylinder and has an

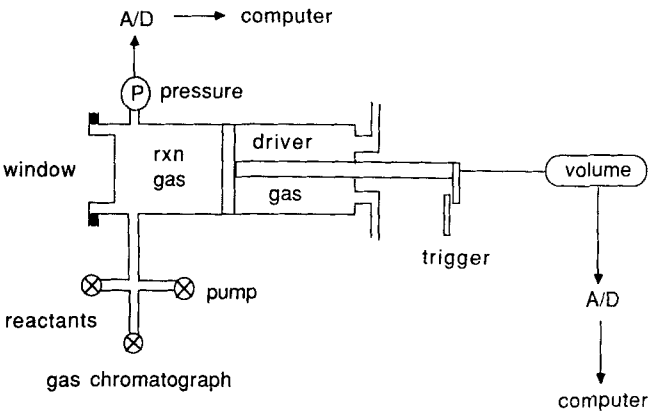

Figure 1. Piston reactor used to compressively heat reactant gases.

inside diameter of 10 cm; a substrate or window closes one end of the cylinder. A piston and rod assembly slides inside the cylinder forming a gas tight seal; a Teflon coating on the interior cylinder surface lubricates the piston seals. Heaters maintain all wall surfaces at a constant temperature (T_w). Any T_w between 25 and 200°C is possible, although 200°C is typical. A pressure transducer (Teledyne-Tabler model 2415; 0–345 kPa) measures the transient gas pressure. A series of pulleys and nonstretch cord instantaneously record the total volume of the reaction gas. During an experiment, a Data Translation analog/digital converter (model 2801A) acquires the pressure and volume transients and stores the data in a microcomputer. Since the piston speed is less than 10 m/s and the total gas pressure never exceeds 267 kPa (2,000 torr), the ideal gas law is applicable, and the product of pressure and total volume is proportional to the transient gas temperature $T_m(t)$. $T_m(t)$ is a mean temperature for the gas as a whole because it encompasses hot gas in the center of the reactor as well as cooler gas near the walls. The driver gas and the mechanical trigger control the motion of the piston. The driver is typically argon at 136 kPa (5 psig). The mechanical trigger holds the piston in place until the experiment is ready to begin.

Operation begins with the piston fully extended and held in place by the mechanical trigger. The cylinder is evacuated and then filled with $\approx$13.3 kPa (100 torr) of the gas mixture (typically, 1% SiH_4 in Ar); all valves are then closed. Pulling the mechanical trigger releases the piston and starts data acquisition. The pressurized argon forces the piston to move down the cylinder, fully compressing the gas mixture in less than 100 ms. At first, the rate of work done on the gas is greater than the instantaneous heat loss rate, and the gas rapidly heats. As the pressure of the reactant gas rises, the piston slows to a stop, and the rate of temperature rise falls to zero. At this time, $T_m(t)$ is approximately twice the starting temperature (500K $\rightarrow$ 1,000 K). Silane homogeneously pyrolyzes at this temperature. If mass transport to the reactor walls were fast enough to overcome particle formation, then the unstable intermediates could deposit film.

The silane employed in these experiments is VLSI grade from Mattheson; the He, H_2, and Ar have purities of 99.9999%, 99.9995%, and 99.999%, respectively. Gas mixtures are vendor-supplied or prepared manometrically in the reactor. A Hewlett-Packard 5790 gas chromatograph with a thermal conductivity

detector provides an analysis of the products of an experiment (H_2, SiH_4, and Si_2H_6). The gas chromatograph uses a carrier gas (Ar or He) that is the same as the diluent employed in the experiment. A Porapak N column at 125°C separates SiH_4 from H_2 and Si_2H_6. During optical measurements, a quartz window replaces the substrate on the reactor. A fast photodiode (EG&G SGD-100A) records the transient emission of visible light. For spectral analysis at 2 ms intervals, we use a Jarrel-Ash spectrograph and a Princeton Applied Research optical multichannel analyzer (OMA). The OMA is a model 1463 with an intensified detector (model 1420); the time constant of the intensified detector is ~2 ms. The spectrograph uses a 50 μm entrance slit and is equipped with a grating with 300 grooves/mm and a 300 nm blaze. There is no lens-focusing system for fear that vibration from the closing piston would unfocus the optics. Consequently, although the spectral resolution of the OMA system is generally less than 1 nm, the low intensities from the reactor limit spectral resolution to 30 nm.

Results

Two typical compressions using silane appear in Figure 2. The initial conditions for each experiment appear in the caption. Note that the peak T_m is roughly the same in both experiments. Morrison and Reimer (1987) have shown that the sharpness of the peak T_m is largely due to the rebound of the piston (expansion cooling). Figure 3 shows the conversion as a function of peak T_m for 1% mixtures of SiH_4 in Ar and He. The initial concentration of reactant is 1 mol %, and the gas analyses are accurate to 0.01 mol % for SiH_4 and 0.05 mol % for Si_2H_6. The best fit and predicted conversions appearing in the graphs are discussed below. Figure 4 shows the conversion of three different mixtures as a function of peak T_m: 1% Si_2H_6, 1% SiH_4, and 1% SiH_4 + 10% H_2. Note that the conversions in both figures are very high. For a given peak T_m, the conversion increases in the following manner: SiH_4 and H_2 in Ar < SiH_4 in Ar < Si_2H_6 in Ar.

The product of all piston experiments with detectable silane conversion is silicon soot and H_2; higher silanes do not appear. No obvious films have formed over the course of over 200 experiments. Soot forms when T_m exceeds 800 K. Changing the initial

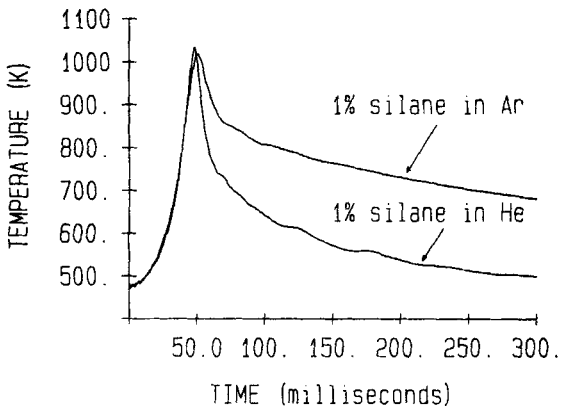

Figure 2. Typical compressions of mixtures of 1% silane in noble gas.

The initial pressure (P_i) for the helium experiment is P_i = 20.0 kPa; for the argon experiment, P_i = 26.7 kPa. For both experiments, the initial temperature = T_w = 475 K and the driver pressure = 136 kPa.

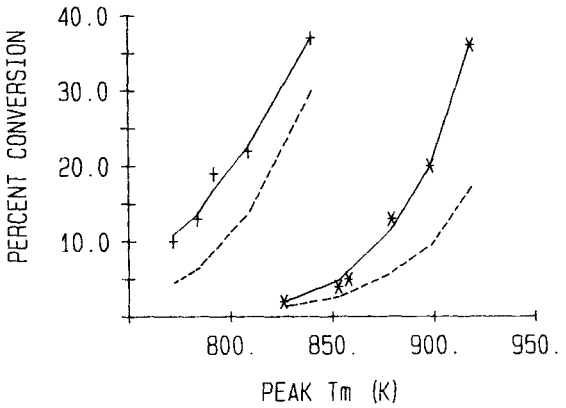

Figure 3. Conversion of SiH_4 vs. peak T_m for two gas mixtures.

* = 1% SiH_4 in Ar and + = 1% SiH_4 in He. ----, predictions using experimental kinetics found in Newman et al. (1979), A_n = 2.14 × 10^{13} s^{-1} and E_n = 220 kJ/mol (52.7 kcal/mol); ——, best fits. For the Ar data, the activation energy is 243 kJ/mol and the preexponential is 8.67 × 10^{14} s^{-1}; for the He data, the values are 163 kJ/mol and 2.06 × 10^{10} s^{-1}.

concentration of silane does not prevent sooting (0.02% to 1% SiH_4 in Ar; 1% SiH_4 in He). Diluting the silane with H_2 does reduce the production of soot but does not eliminate it (1% SiH_4 + 10% H_2 in Ar; 0.5% SiH_4 + 50% H_2 in Ar). There are no conditions where SiH_4 (or Si_2H_6) pyrolyzes without forming detectable soot.

Since no detectable film or higher silanes form, we may assume all of the silane pyrolyzes to soot. In some cases, the amount of soot is so small and widely dispersed that an optical microscope is necessary to detect the particles. The particles are usually orangish brown in color, but are white when the conversion is about 1%. The white color may be due to oxidation of the particles after they are exposed to air. {Mass spectrometry on the reaction shows no significant air leaks, although it does detect argon slowly leaking through the piston seals [≈0.66 Pa · L/s (5 mtorr · L/s)]. As a result, the background O_2 contamination is on the same order of magnitude as the Ar gas purity: 10 ppm.} Scanning electron microscopy shows that the particles are typically less than 1 μm in diameter and fairly monodisperse in size. The soot also collects most heavily on the

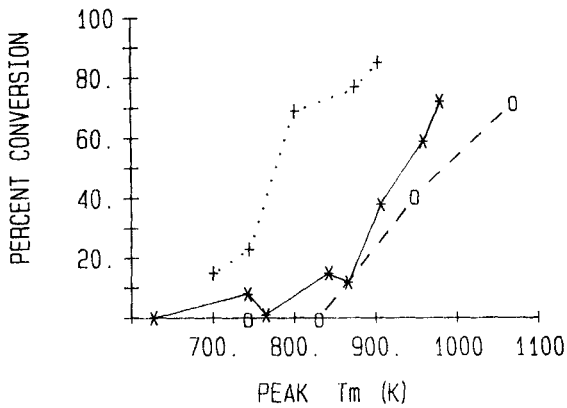

Figure 4. Conversion of reactant for a variety of gas mixtures.

The abscissa is the peak T_m in each experiment, and the diluent is argon. + = 1% Si_2H_6, * = 1% SiH_4, and 0 = 1% SiH_4 + 10% H_2.

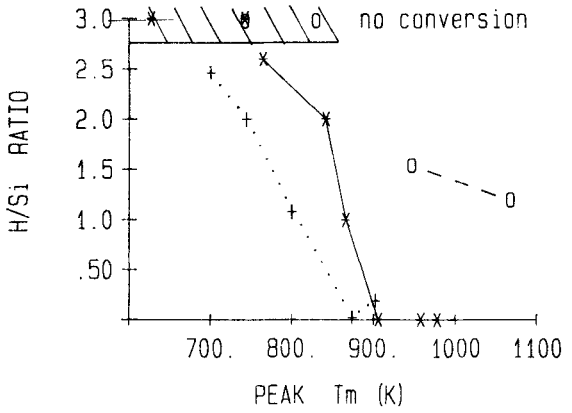

Figure 5. Hydrogen to silicon ratio (H/Si) for silicon soot particles.

The abscissa is the peak T_m in each experiment, and the diluent is argon. + = 1% Si_2H_6, * = 1% SiH_4, and 0 = 1% SiH_4 + 10% H_2.

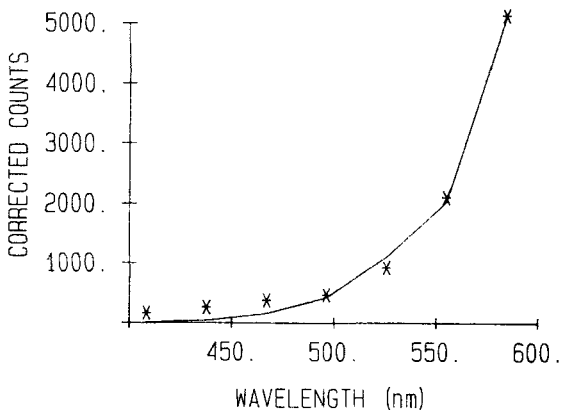

Figure 7. Intensity as a function of wavelength at the maximum intensity.

The solid line is a fit using a black body temperature of 1,098 K.

coldest surfaces of the reactor even though these surfaces are no more than 10–20°C colder. Because there is only 1% reactant initially, each experiment generates too little soot for chemical analysis. Using higher concentration of SiH_4 (10%) reduces the maximum temperature obtainable and thus does not significantly increase the amount of soot produced. However, a mass balance on the reactor does yield an average hydrogen to silicon ratio (H/Si) for the soot (Figure 5). A higher peak T_m produces particles with less hydrogen; Si_2H_6 pyrolysis produces particles with a lower average H/Si than SiH_4 pyrolysis.

Soot is not the only product of the silane decomposition—visible light is emitted. Other authors also have noted that the pyrolysis of silane produces light (Deutsch, 1979; Jasinski and Estes, 1985; O'Keefe and Lampe, 1983). The light intensity (I_{tot}) is a function of time as shown in Figure 6. Both the photodiode and the OMA confirm that I_{tot} has a timescale roughly equivalent to the timescale of changes in $T_m(t)$. The maximum intensity increases nonlinearly with peak T_m. Other experiments show that the integral of $I_{tot}(t)$ over time is proportional to the initial concentration of silane [for a given $T_m(t)$ history and concentrations less than 1%].

Simultaneous spectral and temporal analysis of this light using the OMA shows that the radiation varies smoothly with wavelength and time. Spectral analysis covers the region between 400–600 nm since this region contains some interesting spectral features (Deutsch, 1979). Figure 7 shows a representative spectrum; the resolution of the spectrum is about 30 nm. No sharp features appear at 1 nm resolution (although the sensitivity of the OMA is 30 times smaller at this resolution). The normalized shape of this spectrum is similar to black body radiation. Near the peak temperature, the ratio $I(\lambda_1, t)/I(\lambda_2, t)$ is independent of time for any pair of wavelengths (λ_1, λ_2) although the total intensity declines after the peak T_m. Consequently, we analyze the spectrum near the peak emission where the signal-to-noise is the greatest.

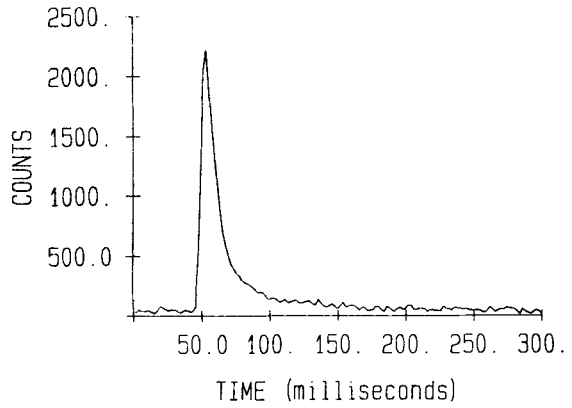

Figure 6. Total intensity of visible light as a function of time.

Discussion

Silane conversion

The trends in conversion seen in Figures 3 and 4 reflect chemical aspects of the compression experiment. In Figure 4, adding H_2 to the SiH_4-Ar mixture chemically changes the pyrolysis by promoting the reverse reaction: $SiH_2 + H_2 \rightarrow SiH_4$; consequently, there is less pyrolysis and less conversion. However, even in a large excess of H_2 (100:1), conversions of $SiH_4 > 10\%$ lead to particles visible to the unaided eye. Hydrogen seems to inhibit SiH_2 formation, but it does not prevent the conversion of SiH_2 to particles. Interestingly, the addition of H_2 to disilane has little effect on the prevention of particle formation. This is also consistent with the interpretation that the pyrolysis of disilane proceeds through the reaction: $Si_2H_6 \rightarrow SiH_2 + SiH_4$. Hence, hydrogen dilution has no effect on the reverse of this reaction.

Predicting SiH_2 conversions shown in Figure 3 is possible using methods developed by Morrison and Reimer (1987). To review, this method requires integrating the equation $d\eta/dt = -k(T, P)\eta$ over the total volume of gas at each point in time (η = total moles of SiH_4 in reactor). Ignoring any pressure fall-off effects [$k(T, P) \rightarrow k(T)$ only] and assuming $T(x, y, z, t) = T_m(t)$ over the whole volume yields $\eta/\eta_o = \exp\left[-\int k(T_m)\, dt'\right]$ integrated over a given compression. Using $T_m(t)$ underestimates the actual temperature and conversion. To compensate for this, we multiply $T_m(t)$ by a known factor determined in other experiments using reactions with known kinetic parameters. Experiments using cyclopropane have determined that these correction factors are 1.05 for Ar experiments and 1.175 for He experiments. Once $T_m(t)$ is corrected, the instantaneous rate constant is calculated, and the conversion is determined.

These correction factors generally work when the compression yields conversions of less than 40%. Higher conversions require stronger compressions whose complicated behavior is not well described by the simple analysis above. Consequently, we will only discuss the low conversion data (<40%).

Of all the silane pyrolyses described in the literature, the conditions in the shock tube experiments of Newman et al. (1979) are the most similar to the peak conditions in the piston reactor. The shock tube conditions are: 1% SiH_4 in Ar, temperatures of 1,035–1,184 K, total pressures of ≈533 kPa (4,000 torr), and conversions of 4–60%. The peak conditions in the piston reactor are: 1% SiH_4 in noble gas, 800–1,050 K, total pressures of ≈267 kPa (2,000 torr) and conversions of 0–80%. Therefore, the calculations in Figure 3 (dashed line) use the *experimental* Arrhenius parameters of Newman et al. (1979) to predict the amount of SiH_4 conversion. The predictions of the SiH_4 data do not fit the data well at all. The best fit on the Ar data yields an activation energy of 243 kJ/mol (58.0 kcal/mol) and a preexponential factor of $8.67 \times 10^{14}\ s^{-1}$; the corresponding best fit values for the He data are 163 kJ/mol (39.0 kcal/mol) and $2.06 \times 10^{10}\ s^{-1}$. Since SiH_4 is in its pressure fall-off regime, using the shock kinetics should overestimate the conversion predicted for the lower pressure piston reactor. This clearly does not explain the deviations shown in Figure 3. The large difference in activation energy for the He and Ar data is also very bothersome. Some other chemical process in the piston reactor has augmented the expected conversion.

Particle emission

The source of the visible radiation is largely due to the incandescence of the soot particles. The flux of photons of wavelength λ from a particle $[B(\lambda,T_p)]$ at a temperature $T_p(K)$ is

$$B(\lambda, T_p) = \frac{\epsilon(\lambda)C_1}{\lambda^4}\left[\exp\left[\frac{C_2}{\lambda T_p}\right] - 1\right]^{-1}\Delta\lambda \qquad (4)$$

where $\epsilon(\lambda)$ is the spectral emissivity, $C_1 = 1.884 \times 10^9$ m/s, $C_2 = 1.439 \times 10^{-2}$ m · K, and $\Delta\lambda$ = wavelength interval (in meters). $\epsilon(\lambda)$ is a function of particle size and optical properties. As a first approximation, we assume that the particles are smaller than the wavelength of light observed (400–600 nm). Rayleigh extinction theory (Rawlins et al., 1984) predicts

$$\epsilon(\lambda) = \frac{6\pi[c]\,l}{N_A \rho_m}\frac{E\{n,k\}}{\lambda} \qquad (5)$$

where $[c]$ is the number density of scatters, l is the path length, N_A is Avogadro's number, and ρ_m is the molar density of the particle. $E\{n,k\}$ is a function of the index of refraction (n) and the extinction coefficient (k) of the bulk material of the scatterers:

$$E\{n,k\} = \frac{6nk}{[n^2 - k^2 + 2]^2 + 4n^2k^2} \qquad (6)$$

Previous investigators (Murthy et al., 1976; van den Brekel and Bollen, 1981; Wu and Flagan, 1987) have determined that the soot particles are crystalline for temperatures above 900–1,000 K. Therefore, the crystalline silicon values for n and k are most appropriate and appear in Table 1 (Palik, 1985). [The values of n and k for amorphous hydrogenated silicon do not significantly change the $\epsilon(\lambda)$ calculation.] Since the measured intensities $I(\lambda)$ are proportional to $B(\lambda, T_p)$, a nonlinear fit of Eq. 4 to $I(\lambda)$ determines the temperature of the particles. (In principle, it is possible to determine the number density of particles from Eq. 4 also. In practice, however, this measurement requires an absolute calibration of the OMA which has not been performed.)

Table 1. Estimated Values for $\epsilon(\lambda)$ for Particles of Crystalline Silicon

λ nm	n	k	$\epsilon(\lambda)/\epsilon \times$ 409 nm
409	5.349	0.313	1.00
438	4.831	0.185	0.73
467	4.495	0.120	0.54
496	4.320	0.073	0.34
526	4.177	0.053	0.26
555	4.073	0.032	0.16
584	3.983	0.030	0.15

The results of fitting $I(\lambda)$ to $B(\lambda, T_p)$ yields the particle temperatures (T_p) shown in Table 2. In nearly all cases, T_p agrees reasonably well with the corrected peak T_m. Note that the values of peak T_m shown in Table 2 correspond to conversions in excess of 50%, and therefore, we did not expect the corrected peak T_m and T_p to agree so closely. This result is consistent with detailed mass and energy balances on a particle, despite the fact that the "condensation" of silicon from silane is exothermic by about 25–34 kJ/mol. At the temperatures and pressures found in the reactor, the conductive flux of heat from Ar (or He) completely dominates all other effects, and T_p should always be equal to the local gas temperature (T_g).

Despite the above evidence, a problem remains. Careful examination of Figure 7 using a chi-squared test (Bevington, 1969) shows that the black body model fits the data well at the red end of the spectrum but deviates significantly at the blue end. One possible hypothesis is that there is a distribution of particle temperatures. For example, a small fraction of the particles may be at some high temperature and thus augment the blue end of the spectrum. This may occur if the heat of reaction on the soot particle were significantly more exothermic than assumed in the heat balance. We have fit the data using a model with two particle temperatures, and the results are compared to the one temperature model in Table 3. (A reduced chi-squared of 1.5 indicates a statistically significant fit.) The two temperature model reduces chi-squared, but it yields one temperature well above the boiling point of silicon (3,500 K). This is clearly unrealistic.

A nonblack body source of radiation in addition to incandescing particles can explain the deviations in the one temperature fit. In shock tube studies of sooting in hydrocarbons, Rawlins et

Table 2. Particle Temperature from Spectral Analysis

Sample	Peak T_m	Corrected T_m	Particle Temp.	Conversion
Silane	1,020 K	1,070 K	1,030-1,070 K	72%
in Ar	1,170 K	1,230 K	1,240 K	91%
Silane	940 K	1,100 K	1,190-1,250 K	53%
in He	1,030 K	1,210 K	1,270-1,330 K	71%
Disilane	930 K	980 K	900-1,000 K	>80%
in Ar	1,030 K	1,080 K	950-1,000 K	>80%

Table 3. Comparison of One Temperature and Two Temperature Fits

Fit	Cold T_p K	Hot T_p K	Fraction Hot, $\times 10^{-9}$	Reduced χ^2
One Temp.	1,096	—	0.0	18.20
Two Temp.	1,003	4,060	0.25	8.43

al. (1984) have observed the emission of visible light from two different sources. In the stages of pyrolysis prior to the formation of a particle embryo, molecular species emit visible light in a nearly continuous spectrum. The time scale of this event is microseconds. After formation, the embryo grows into a particle and incandesces at the local gas temperature. The time scale of this event is milliseconds. As mentioned before, the OMA uses a time exposure of 2 ms, and the OMA spectrum may contain both emissions from molecular species and particle incandescence.

Surface growth model

If one assumes that the only loss mechanism for SiH_4 is through SiH_2 formation, the piston results would indicate a significant deviation from literature kinetics. Particle growth models currently available all assume the rate limiting step is SiH_2 formation (Wu et al., 1987, 1988). We have developed the surface growth model to overcome this limitation (Figure 8). The pyrolytic reactions of silane form SiH_2 at high temperatures. If H_2 is present, it inhibits the pyrolysis by promoting the reverse reaction $H_2 + SiH_2 \rightarrow SiH_4$. SiH_2 undergoes reactive nucleation and quickly forms a soot embryo. The blue continuum radiation may originate from the embryos. This embryo has physical properties that bridge the gap between $SiH_2(g)$ and the solid soot particle. Fast coagulation of embryos generates a silicon soot particle. Once a particle forms, surface growth from SiH_4 becomes possible. The activation energy (E_s) of such a surface reaction is hard to guess, since the E_s of the heterogeneous reactions of SiH_4 varies between $\approx$71 kJ/mol on a clean (111) surface (Farrow, 1974) and $\approx$210 kJ/mol on a hydrogenated silicon surface (Beers and Bloem, 1982). The relative amounts of SiH_4 consumed via reactive nucleation and surface growth are also unknown. As the surface reactions occur, various other processes proceed. The particles slowly coagulate (which reduces the number of particles in favor of larger diameters), the particles radiate heat and light at the local gas temperature, and particles transport to the reactor walls by diffusion or by thermophoresis. These processes cause the size distribution of the particle diameters, the black body radiation, and the particle deposition on cold reactor walls.

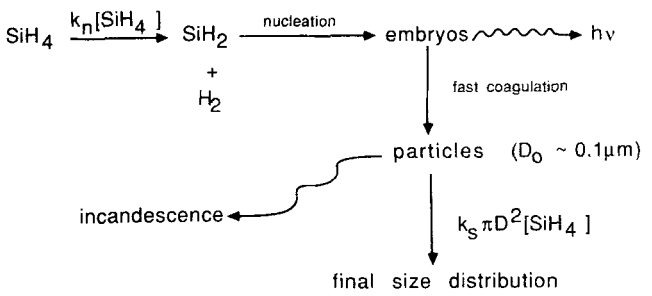

Figure 8. Proposed surface growth model.

We have constructed a semiquantitative model to test the plausibility of this hypothesis. Due to the uncertainties in the kinetics of the surface reactions and the detailed physics of nucleation, the surface growth model is necessarily very simple and is not expected to reproduce the piston results exactly. Despite the following simplifications, the model is fairly successful.

The model assumes SiH_2 formation is the rate limiting step for new particle formation and has the kinetics $k_n(T) = A_n \exp(-E_n/RT)$. The model further assumes that all of the new particles are born with a uniform diameter (D_0) on the order of 0.1 μm. This is the typical size produced in a spontaneously nucleating seed reactor (Alam and Flagan, 1986). This assumption hides all of the details of the nucleation and embryo coagulation processes, but it is a necessary simplification to keep the problem tractable. Please note that the surface area per gram of particles increases as the mean particle diameter decreases, so that choosing a uniform diameter is probably an underestimate of the particle surface area and the relative importance of surface growth. After a particle is born, impinging SiH_4 molecules decompose on its surface with an efficiency given by $k_s(T) = A_s \exp(-E_s/RT)$. Coagulation of the particles is ignored because their number density is not high enough to make that process significant. To demonstrate this, consider that the kinetics of Newman et al (1979) predict that 6.3% of the available SiH_4 is converted to SiH_2 in 1 ms at 1,000 K. If the SiH_4 partial pressure is 20 torr (2.7 kPa), this conversion is equivalent to 1.2×10^{16} SiH_2 per cm^3. If this mass condenses to 0.1 μm particles, the particle number is about 5×10^8 cm^{-3}. The results of Wu and Flagan (1987) predict that the time constant for self-coagulation at this concentration is about one second.

The following dimensional equations describe the surface growth model:

$$\eta_0 - \eta = \rho_m \sum_{i=1}^{j} N_i \frac{\pi D_i^3}{6} \qquad i \le j \tag{7}$$

$$\frac{d}{dt}\left[\rho_m \frac{\pi D_i^3}{6}\right] = k_s(T) \frac{v(T)}{4} \pi D_i^2 C \qquad i \le j \tag{8}$$

$$\frac{dN_i}{dt} = 0 \qquad i < j \tag{9a}$$

$$\rho_m \frac{\pi D_0^3}{6} \frac{dN_i}{dt} = k_n(T)\eta \qquad i = j \tag{9b}$$

where

η_0 = initial number of moles of silane in reactor
$\eta(t)$ = number of moles of silane at the time t
ρ_m = molar density of solid silicon
D_i = diameter of particles born at time t_i
N_i = total number of particles born at time t_i
$v(T)$ = thermal velocity of SiH_4
C = concentration of silane

Time (t) appears in the equation through the time index (j) and the time step (h): $t_j = jh$. Equation 7 is a total mass balance, Eq.

8 is a mass balance on an individual particle, and Eq. 9a and 9b are the formation rates for old and new particles, respectively. Equation 9a accounts for the fact that N_i for old particles do not change. Nondimensionalizing the equations yields

$$F(t) = 1 - \left(\frac{\rho_m \pi D_0^3}{6\eta_0}\right) \sum_{i=1}^{j} N_i \Delta_i^3 \quad i \le j \tag{10}$$

$$\frac{d\Delta_i}{dt} = \frac{A_s C_0}{2\rho_m D_0} \frac{v(T)}{V(t)} \exp\left(-\frac{E_s}{RT}\right) \cdot F(t) \quad i \le j \tag{11}$$

$$\frac{dN_i}{dt} = 0 \quad i < j \tag{12a}$$

$$\frac{dN_i}{dt} = \frac{6\eta_0 A_n}{\pi \rho_m D_0^3} \cdot \exp\left(-\frac{E_n}{RT}\right) \cdot F(t) \quad i = j \tag{12b}$$

where $\Delta_i = D_i/D_o$, $F(t) = \eta(t)/\eta_0 = V(t)C/V_0\ C_0$, and $V(t)$ = total volume of the reactor at time t.

The set of equations are solved with a fourth order Runge-Kutta method. The parameters in the model are A_s, E_s, A_n, E_n, and D_0. The values for A_n and E_n come from Newman et al. (1979) and will not be varied. Of the remaining three parameters, A_s and D_0 influence $F(t)$ only through Eq. 11. (The D_0's in Eq. 10 cancel the D_0's in Equation 12b.) Furthermore, A_s and D_0 are not independent since they appear as a ratio. Therefore, the surface growth model has only two independent parameters: A_s/D_0 and E_s. The simulations will use values for A_s and E_s that are similar to the results of Farrow (1974): $A_s = 5.45$ and $E_s = 71$ kJ/mol (17 kcal/mol).

Figure 9 shows two simulations of 1-$F(t)$ for a compression of 1% SiH_4 in Ar: one simulation uses surface growth ($A_s/D_0 > 0$) and the other does not ($A_s/D_0 = 0$). The simulation parameters appear in the caption. The activation energy for nucleation (E_n) is fairly high (221 kJ/mol), and so 1-$F(t)$ does not change significantly after 60 ms if there is no surface growth. The addition of surface growth with a low activation energy shows that significant SiH_4 depletion can occur in the tail of $T_m(t)$. Figure 9 shows that the conversion continues to rise for $t > 300$ ms. We account for the conversion at times longer than 300 ms by extrapolating $T_m(t)$ assuming that ln $[T_m(t) - T_w]$ is proportional to time and solving Eq. 10–12 using the extrapolated $T_m(t)$. Figure 10 shows some results from such calculations using various D_0. The * are Ar data, the + are He data, and the lines represent simulation results using $D_0 = 0.05$ μm, 0.1 μm, and ∞. Note that the $D_0 \rightarrow \infty$ case represents no surface growth ($A_s = 0$) and therefore is identical to the predictions in Figure 3. The simulation using $D_0 = 0.05$ μm (50nm) fits the Ar data very well and fits the He data well for conversions less than 20% (Figure 10). Considering the simplicity of the model and the large differences in apparent activation energy for the He and Ar data (163 kJ/mol and 243 kJ/mol, respectively), the model is remarkably successful. Figure 11 shows other results for various values of E_s.

The above model is consistent with shock tube studies of silane pyrolysis. Although particles have been observed in very hot shocks (Steinwandel and Hoeschele, 1985; Hoschele et al., 1986), other investigators (Newman et al., 1979) tacitly assume that particles do not interfere with the measurement of k_n (SiH_2

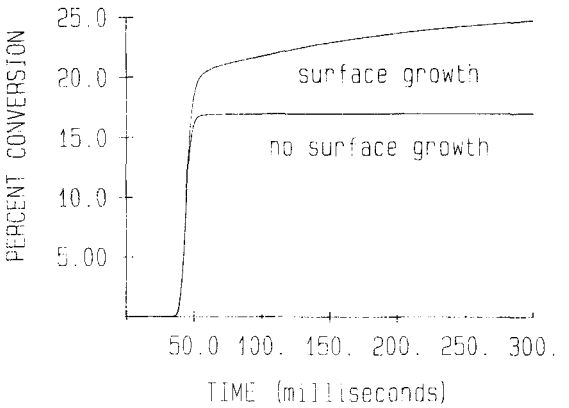

Figure 9. Two simulations of conversion as a function of time using the surface growth model.

The experiment is a compression of 1% SiH_4 in Ar with a peak T_m of 918 K. The parameters in the model are $D_0 = 0.1$ μm and $E_s = 7.10$ kJ/mol (17.0 kcal/mol). For the no surface growth case, $A_s = 0$; with surface growth, $A_s = 5.45$.

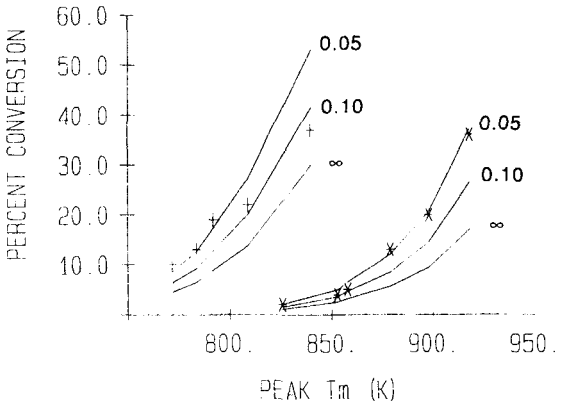

Figure 10. Predicted conversion as a function of peak T_m for various values of D_0.

* = Ar data, + He data, and the solid lines are simulated results. The simulation parameters are: $A_s = 5.45$ and $E_s = 71.0$ kJ/mol (17.0 kcal/mol). The labels refer to values of D_0 (in μm) used in the simulations. Note that $D_0 \rightarrow \infty$ is equivalent to the no surface growth case ($A_s = 0$).

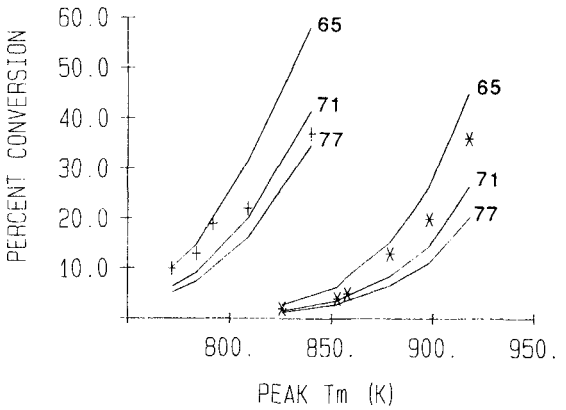

Figure 11. Predicted conversion as a function of peak T_m for various values of E_a.

* = Ar data, + = He data, and the solid lines are simulated results. The simulation parameters are: $A_s = 5.45$ and $D_0 = 0.1$ μm. The labels refer to values of E_a (in kJ/mol) used in the simulations.

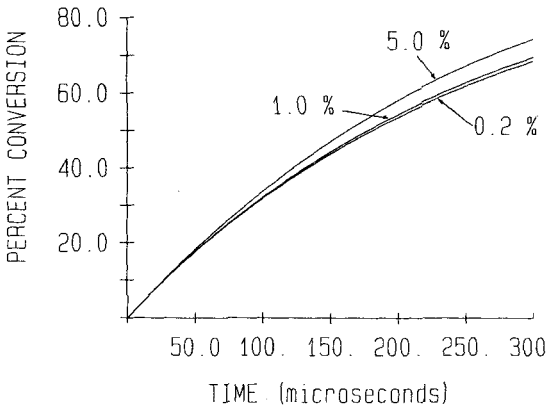

Figure 12. Predicted conversion as a function of time for a shock experiment using various values of silane concentration.

The simulation parameters are: temperature = 1,182 K; A_s = 5.45; E_s = 71.0 kJ/mol (17.0 kcal/mol); and D_o = 0.05 μm.

formation) in low temperature shocks ($T < 1{,}200$ K). The surface growth model verifies this assumption. Using the best fit parameters from Figure 10 and a silane concentration of C_0 = 1%, simulations of a 300 μs shock at T = 1,182 K predict the conversion is 71.0% when surface growth is present and 68.5% when surface growth is absent. This small difference is well within experimental error and leads to the conclusion that the kinetics of the shock experiment are largely unaffected by surface growth. This conclusion is only partly correct, however. If C_0 is above 1%, the simulated conversion deviates strongly from apparent first order kinetics (Figure 12). This arises because C_0 affects Eq. 11 the same way that A_s/D_0 does. Since Newman et al have done experiments using C_0 between 0.1% and 1%, they would not have seen the deviation from first order kinetics. We must predict, therefore, that the shock tube experiment generates silicon soot but that surface growth plays very little role in the shock kinetics as long as $C_0 < 1\%$. The presence of soot in the shock experiment also explains the isotope scrambling observed (Newman et al., 1979). HD can be produced in the nucleation reaction or on the growing surface of the soot particles without involving any free radical mechanism.

Conclusions

In experiments with SiH_4, the piston reactor successfully pyrolyzes SiH_4 and precipitates silicon soot under most experimental conditions. The kinetics of reactive nucleation are so fast that there is virtually no loss of intermediates by transport to the walls. These experiments have revealed some interesting features of particle nucleation. The hydrogen content of the particles is highest at the lowest reaction temperatures. The emission of visible light accompanies the sooting reactions. There are two sources for the visible light: 1) silicon particles incandescing at the local gas temperature; and 2) a nonblack body radiating over a broad spectrum. The particles form at relatively mild conditions and therefore appear early in the pyrolysis. Because these particles remain relatively hot in the tail of $T_m(t)$, SiH_4 reacts with them, and their presence adds a second loss mechanism to nucleation. A simple surface growth model can account for the additional conversion seen in the piston experiments. The absence of such a temperature tail in a shock tube experiment vastly reduces the role of surface growth in that experiment.

Acknowledgment

Grants from Xerox, the National Science Foundation (MSM84-51234), the Universitywide Energy Research Group, and the Chancellor's Patent Fund have supported this work. The authors also gratefully acknowledge the San Francisco Laser Lending Center for providing the optical multichannel analyzer.

Notation

$B(\lambda,T_p)$ = black body function, photons/m^2 · s
C = concentration of silane, mol/cm^3
$[c]$ = number density of particles, cm^{-3}
C_1 = a constant = 1.884×10^9 m/s
C_2 = a constant = 1.439×10^{-2} m · K
D_i = diameter of ith particle, cm
D_0 = initial diameter of particle before surface growth, cm
E_n = activation energy of SiH_2 formation, J/mol
E_s = activation energy of the surface reaction, J/mol
$E\{n,k\}$ = extinction function in Eqs. 5 and 6
$F(t)$ = relative fraction of silane remaining = η/η_0
h = time step size, s
$I_{tot}(t)$ = total intensity of emitted light (arbitrary counts)
$I(\lambda,t)$ = intensity of emitted light at a wavelength λ (arbitrary counts)
j = time index = t/h
k = extinction coefficient
$k(T)$ = first order rate constant, s^{-1}
k_n = rate constant of SiH_2 formation, s^{-1}
k_s = reaction efficiency of surface growth on a particle
l = optical path length, cm
n = index of refraction
N_A = Avogadro's number = 6.02×10^{23} mol^{-1}
N_i = number of particles of size D_i
P_{crit} = critical pressure at which nucleation occurs, torr (Pa)
P_i = initial pressure, kPa
R = ideal gas constant = 8.31 J/mol · K
t = time, s
T = temperature, K
T_g = local gas temperature, K
$T_m(t)$ = mean gas temperature, K
T_p = particle temperature, K
T_r = reference temperature, K
T_w = wall temperature, K
v = mean thermal velocity of silane, cm/s

Greek letters

Δ_i = dimensionless diameter of particles = D_i/D_0
$\epsilon(\lambda)$ = spectral emissivity
λ = wavelength, m
$\Delta\lambda$ = wavelength interval or bandwidth, m
η = total moles of silane in reactor, mol
η_0 = initial number of moles of silane in reactor, mol
ρ_m = molar density of the solid particle, mol/cm^3

Literature Cited

Alam, M. K., and R. C. Flagan, "Controlled Nucleation Aerosol Reactors: Production of Bulk Silicon," *Aerosol Sci. Tech.*, **5**, 237 (1986).

Beers, A. M., and J. Bloem, "Temperature Dependence of the Growth Rate of Silicon Prepared Through Chemical Vapor Deposition from Silane," *Appl. Phys. Lett.*, **41**, 153 (1982).

Bevington, P. R., *Data Reduction and Error Analysis for the Physical Sciences*, McGraw-Hill, New York (1969).

Cannon, W. R., S. C. Danforth, J. H. Flint, J. S. Haggerty, and R. A. Marra, "Sinterable Ceramic Powders from Laser-Driven Reactions: I. Process Description and Modeling," *J. Amer. Ceram. Soc.*, **65**, 324 (1982a).

Cannon, W. R., S. C. Danforth, J. S. Haggerty, and R. A. Marra, "Sinterable Ceramic Powders from Laser-Driven Reactions: II. Powder Characteristics and Process Variables," *J. Amer. Ceram. Soc.*, **65**, 330, (1982b).

Deutsch, T. F., "Infrared Laser Photochemistry of Silane," *J. Chem. Phys.*, **70**, 1187, (1979).

Donahue, T. J., and R. Reif, "Low Temperature Silicon Epitaxy Deposited by Very Low Pressure Chemical Vapor Deposition," *J. Electrochem. Soc.*, **133,** 1691 (1986).
Eversteijn, F. C., "Gas Phase Decomposition of Silane in a Horizontal Epitaxial Reactor," *Phillips Res. Rep.*, **26,** 134 (1971).
Farrow, R. F. C., "The Kinetics of Silicon Deposition on Silicon by Pyrolysis of Silane," *J. Electrochem. Soc.*, **121,** 899 (1974).
Herrick, C. S., and D. W. Woodruff, "The Homogeneous Nucleation of Condensed Silicon in the Gaseous Si-H-Cl System," *J. Electrochem. Soc.*, **131,** 2417 (1984).
Hoschele, J., M. Hauser, and J. Steinwandel, "The Formation Kinetics of Ultrafine a-Si:H Aerosols by Shock Pyrolysis of SiH_4," *Aerosols: Formation and Reactivity*, Int. Aerosol Conf., Berlin, Pergamon, Great Britain (1986).
Hottier, F., and R. Cadoret, "Analysis of Silicon Crystal Growth Using Low Pressure Chemical Vapour Deposition," *J. Cryst. Growth*, **61,** 245 (1983).
Jasinski, J. M., and R. D. Estes, "Laser Powered Homogeneous Pyrolysis of Silane," *Chem. Phys. Lett.*, **117,** 495 (1985).
Jasinski, J. M., B. S. Meyerson, and B. A. Scott, "Mechanistic Studies of Chemical Vapor Deposition," *Annu. Rev. Phys. Chem.*, **38,** 109 (1987).
Morrison, Jr., P. W. and J. A. Reimer, "A Simple Method to Study Gas Phase Reactions," *AIChE J.*, **33,** 2037 (1987).
Murthy, T. U. M. S., N. Miyamoto, M. Shimbo, and J. Nishizawa, "Gas Phase Nucleation During the Thermal Decomposition of Silane in Hydrogen," *J. Cryst. Growth*, **33,** 1 (1976).
Neudorfl, P., A. Jodhan, and O. P. Strausz, "Mechanism of the Thermal Decomposition of Monosilane," *J. Phys. Chem.*, **84,** 338 (1980).
Newman, C. G., H. E. O'Neal, M. A. Ring, F. Leska, and N. Shipley, "Kinetics and Mechanism of the Silane Decomposition," *Int. J. Chem. Kinet.*, **11,** 1167 (1979).
O'Keefe, J. F., and F. W. Lampe, "Spectroscopic Detection of Silylene in the Infrared Multiphoton Decomposition of Silane," *App. Phys. Lett.*, **42,** 217 (1983).
Palik, E. D., *Handbook of Optical Constants of Solids*, Academic Press, Orlando (1985).
Purnell, J. H., and R. Walsh, "Pyrolysis of Monosilane," *Proc. of Royal Soc. A*, **293,** 543 (1966).
Rawlins, W. T., L. M. Cowles, and R. H. Krech, "Spectral Signatures (0.2–5 μm) of Soot Intitation in the Pyrolysis of Toluene Near 2,000 K," 20th Int. Symp. Comb., 879 (1984).
Roth, R. M., K. G. Spears, G. D. Stein, and G. Wong, "Spatial Dependence of Particle Light Scattering in an RF Silane Discharge," *Appl. Phys. Lett.*, **46,** 253 (1985).
Scott, B. A., W. L. Olbricht, B. S. Meyerson, J. A. Reimer and D. J. Wolford, "Homogeneous Chemical Vapor Deposition," *J. Vac. Sci. Technol. A*, **2,** 450 (1984).
Spears, K. G., T. J. Robinson, and R. M. Roth, "Particle Distributions and Laser-Particle Interactions in an RF Discharge of Silane," *IEEE Trans. Plasma Sci.*, **PS-14,** 1979 (1986).
Steinwandel, J., and J. Hoeschele, "Spectroscopic Detection of Particles from Shock Wave Induced Decomposition of SiH_4," *Chem. Phys. Lett.*, **116,** 25 (1985).
van den Brekel, C. H. J., and L. J. M. Bollen, "Low Pressure Deposition of Polycrystalline Silicon from Silane," *J. Cryst. Growth*, **54,** 310 (1981).
White, R. T., R. L. Espino-Rios, D. S. Rogers, M. A. Ring, and H. E. O'Neal, "Mechanism of the Silane Decomposition: I. Silane Loss Kinetics and Rate Inhibition by Hydrogen; II. Modeling of the Silane Decomposition (All Stages of Reaction)," *Int. J. Chem. Kin.*, **17,** 1029 (1985).
Wu, J. J., and R. C. Flagan, "Submicron Silicon Powder Production in an Aerosol Reactor," *Appl. Phys. Lett.*, **49,** 82 (1986).
Wu, J. J., and R. C. Flagan, "Onset of Runaway Nucleation in Aerosol Reactors," *J. App. Phys.*, **61,** 1365 (1987).
Wu, J. J., H. V. Nguyen, and R. C. Flagan, "A Method for the Synthesis of Submicron Particles," *Langmuir*, **3,** 266 (1987).
Wu, J. J., H. V. Nguyen, R. C. Flagan, K. Okuyama, and Y. Kousaka, "Evaluation and Control of Particle Properties in Aerosol Reactors," *AIChE J.*, **34,** 1249 (1988).

Manuscript received Dec. 10, 1987, and revision received Jan. 27, 1989.